Molecular dynamics study of Al implantation in 4H-SiC

Sabine Leroch[1]*, Robert Stella[1], Andreas Hössinger[2], and Lado Filipovic[1]
[1]CDL for Multi-Scale Process Modeling of Semiconductor Devices and Sensors, at the Institute for Microelectronics, TU Wien, 1040 Vienna, Austria
[2]Silvaco Europe Ltd., St Ives, Cambridgeshire, PE27 5JL, United Kingdom
*Email: leroch@iue.tuwien.ac.at

***Abstract*—We have performed a molecular dynamics study of Al-implantation in 4H-SiC while investigating the types of defects produced and their quantity depending on the implantation temperature and dose. The damage to the SiC lattice should be minimized to facilitate the subsequent Al activation during annealing. Using the empirical Gao-Weber potential, together with a recently proposed Morse potential for the Al-SiC interaction, we show that implantation at elevated temperatures considerably reduces the creation of amorphous pockets and extended defect clusters. In a follow-up annealing study we aim to provide a correlation between dose/implantation temperature and the Al activation rate to give guidance for future fabrication of SiC devices.**

***Index Terms*—4H-SiC, Gao-Weber potential, Al-implantation, formation energies of Al in SiC, high-temperature implantation**

I. Introduction

In this work, we study the dose- and temperature-dependent Al-doping of 4H-SiC for the generation of p-doped SiC. The 4H structure is highly technologically relevant and provides the widest band gap (3.26 eV) among the alternative polytypes; these differ only by the stacking sequence of hexagonal closed packed layers in the $\langle 0001 \rangle$ direction. During semiconductor fabrication Al ions (with desired dose and energy) are implanted. Ideally, the dopants are placed at lattice sides, where they are subsequently activated, i.e., they provide free carriers. In reality, the Al ions can occupy any energetically possible position in the SiC structure immediately after implantation. Moreover, the ion bombardment causes a displacement of the native atoms from their locations in the ideal crystal, thereby creating interstitials, vacancies, or groups of defect clusters, up to amorphous pockets. These defects not only impact the conductivity of SiC after activation, but it is also known that C interstitials and vacancies can form stable compounds with Al. This way Al is trapped, such that it is inaccessible for activation [1].

Usually, annealing the crystal at high temperatures can assist to promote the migration (diffusion) of the atoms, i.e., to enable them to cross barriers on the free energy landscape and move them to the next local energy minimum. Since SiC has a low diffusion coefficient, temperatures higher than 2000 K are typically applied during the annealing stage after implantation. This allows to recover single defects, while large defect clusters are often not completely annealed out, thereby constituting defect centers such as D_{II} [2].

Due to the factors mentioned above, a principal goal during SiC doping is to avoid large defect clusters and crystalline damage during implantation, which has been shown to be achievable experimentally by increasing the temperature during the implantation step [3]–[5]. However, the correlation between implantation temperature and dose and the dopant activation efficiency is not fully understood. *Ab-initio* DFT calculations [6], [7] can provide very accurate activation energies, from where diffusivities and diffusion constants of Al in SiC can be deduced. The quantum system offered by *ab-initio* DFT constitutes a perfect emulation model, where the interaction energy of a dopant and a defect, in an otherwise perfect SiC lattice, can be determined. However, realistically, Al diffuses through a distorted crystal structure and simultaneously interacts with many smaller and extended defects in its path. In addition, we need to follow the movement of Al on longer time scales than what is feasible using DFT simulations during implanation and especially during the subsequent annealing step. To shed more light on the formation of defects during the ion implantation process, molecular dynamic (MD) simulations are carried out in this study.

II. Methods

For the MD simulation, the software framework LAMMPS [8] is used, while the OVITO [9] tool is used for subsequent visualization.

A. Interatomic Potentials

For MD simulations, an empirical potential is desired, which is able to physically describe the features of interest within the studied system. The Tersoff [10] and Gao-Weber (GW) [11] potentials are most commonly used for SiC simulations. Both potentials are expanded by a Ziegler-Biersack-Littmark (ZBL) term which models the repulsive forces between the atoms. For the interaction of the Al with the Si and C atoms, the Morse potential, proposed by Dandekar and Shin, is typically used [12]. The Tersoff potential has found very wide application in MD simulations of SiC systems. The GW potential, however, was originally parametrized to reproduce DFT migration and formation energies of self-defects in 3C-SiC [13]–[15]. The migration barriers are especially in good agreement with DFT results, as provided in [16]. The GW potential has thus found many applications in the field of ion-beam induced defects and defect migration [16]–[18].

To facilitate the choice of an existing empirical potential in our study, we analyzed the potentials with respect to their compatibility with the proposed aluminum Morse potential; essentially, we analyzed whether a combination of these potentials is able to describe the diffusion and activation energies of Al in 4H-SiC with sufficient physical accuracy, by comparing against DFT results.

TABLE I
Formation energies (eV) for 4H-SiC calculated using the Gao-Weber and Tersoff potentials, compared to published DFT data.

Defect	Gao-Weber	Tersoff	DFT	Reference
Al_{TSi_k}	5.39	7.90	8.26	[13]
Al_{TC_k}	5.64	5.93	6.12	[13]
Al_{Si}	1.58	5.02	1.36	[13]
Al_{Si}+V_C	3.54	7.76	3.28	[13]
Al_{hex}	3.68	4.87	8.50	[7]
Al_{Si}+Si_{hex}	4.61	17.28	9.20	[6]
Al_{Si}+Si_{TC}	2.96	17.82	7.28	[13]

The migration and the kick-in process of Al in SiC, which subsitutes only for Si in the lattice, is well known [6]. Starting from a neighboring Al interstitial in a hexagonal or tetragonal position, the kick-in proceeds via the formation of a split interstitial with a Si atom. During diffusion, Al migrates preferentially from one tetragonal interstitial side in the cubic layer of 4H-SiC to the neighboring one, passing over a hexagonal interstitial side as a saddlepoint (barrier).

The cut-off distance for the Morse potential (4.5 Å for Si and 3.5 Å for C) was chosen such that the formation energies of Al defects and their compounds are in reasonable agreement with DFT data; moreover, the migration barriers should be close to the DFT results. In Table I, the calculated formation energies are compared with published DFT data. The Tersoff potential tends to greatly overestimate, while the GW potential underestimates, the formation energy for different Al defects.

To validate the migration barrier, the kick-out process of Al from the Al_{Si} to the hexagonal interstitial position Al_{hex} with the assistance of a Si interstitial Si_{TC}, was calculated. The GW potential shows a migration barrier for the kick-out of 3.44 eV which is in reasonable agreement with the DFT data of 4.5 eV [6]. The Tersoff potential, on the other hand, shows practically no kick-out barrier, but a very high kick-in barrier for Al of 12.5 eV, rendering it nearly impossible that a remote Al is accommodated into the SiC lattice during annealing. Since the migration and kick-in barriers are well captured, and in confirmation of former studies [19], we conclude that the GW potential is more suitable to describe the diffusion and activation of Al in SiC.

B. Molecular Dynamics Simulation

A cuboidal SiC block of size 9nm×10nm×21nm shown in Fig. 1 was constructed by stacking hexagonal closed packed layers in the ⟨0001⟩ direction on top of each other. The crystal was first equilibrated in the constant-temperature constant-pressure (NPT) ensemble. In the subsequent implantation step the volume is partitioned into a Newtonian, thermostat, and boundary layer, as visualized in Fig. 1. In the Newton layer only the total energy of the system is kept constant, the thermostat serves as thermal bath and the boundary layer avoids the box moving during implantation. The Al atoms are implanted sequentially with an impinging angle of 7° and a relaxation period between the implantation steps of 10 ps. To avoid an artificial overheating of the system through ion bombardment, the electron/stopping algorithm is applied, which models electronic stopping using an equivalent friction force. By applying the electronic stopping algorithm, one at least conceptually accounts for the fact that in a real system part of the ion-energy is transferred to the electrons of the crystal.

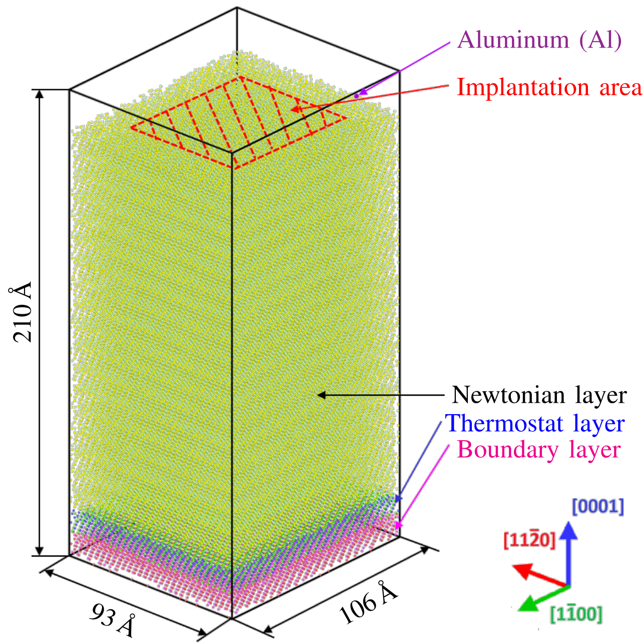

Fig. 1. Model for the MD setup. In the Newtonian layer only the total energy of the system is kept constant, the thermostat serves as thermal bath, and the boundary layer keeps the box static during implantation.

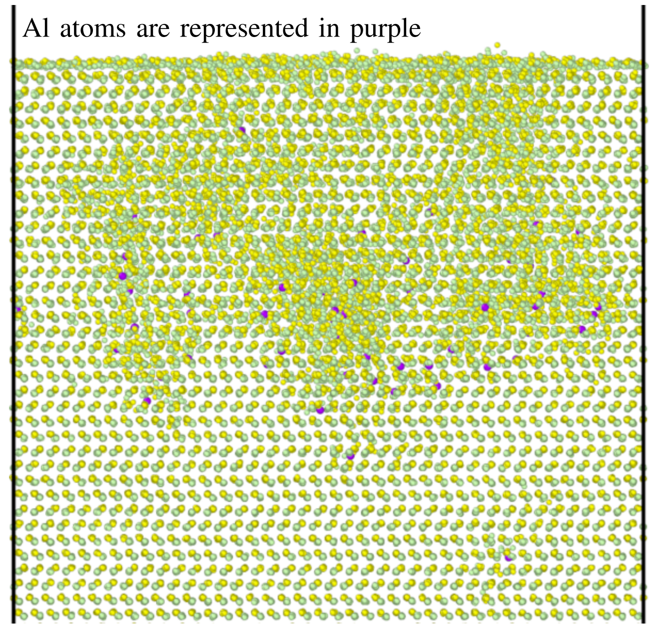

Fig. 2. 4H-SiC structure immediately after implantation of Al.

III. Results and Discussion

In Fig. 2, one can observe the damage in the 4H-SiC structure directly after Al implantation. To investigate the damaged structure further, we used the identify diamond structure (IDS) algorithm from OVITO [9]. IDS automatically marks the groups of atoms which are not in perfect hexagonal or cubic diamond formations. These are groups containing interstitials, antisites, or vacancies; amorphous clusters are likewise identified.

In Fig. 3 the IDS structure for the highest and lowest dose investigated here are shown, when implanting at room temperature and at an elevated temperature of 800 K. For the two tested Al doses (5×10^{13} cm^{-2} and 5×10^{14} cm^{-2}) an improvement with respect to the number of created defects can be observed, when using higher temperatures. Especially the amorphous structures, shown in grey for the high dose in Fig. 3(b), nearly diminishes for implants at 800 K in Fig. 3(d). This effect can be observed more clearly in Fig. 4(b), where the black lines are the results for room temperature implantation and the red lines are for implanatation at 800 K. The effect at lower doses is reduced because, even at these short time scales (i.e., few ns) single defects are annealing out during implantation. As shown in the histogram in Fig. 4(a), most of the defect clusters consist of only one or two defects for the system with an implant dose of 5×10^{13}cm^{-2} at 800 K.

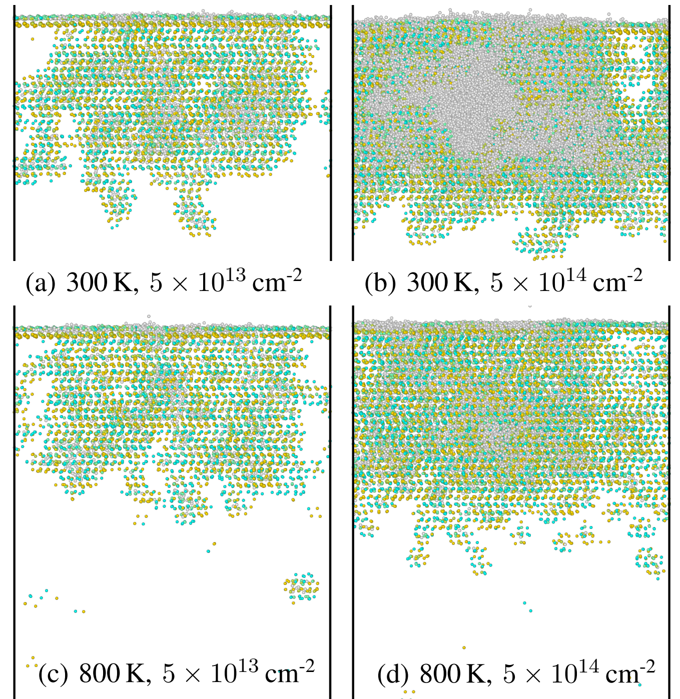

Fig. 3. IDS structures directly after Al implantation for implant doses (a,c) 5×10^{13} cm^{-2} and (b,d) 5×10^{14} cm^{-2}) and temperatures (a, b) 300 K and (c, d) 800 K. The grey patch in (b) represents an amorphous cluster.

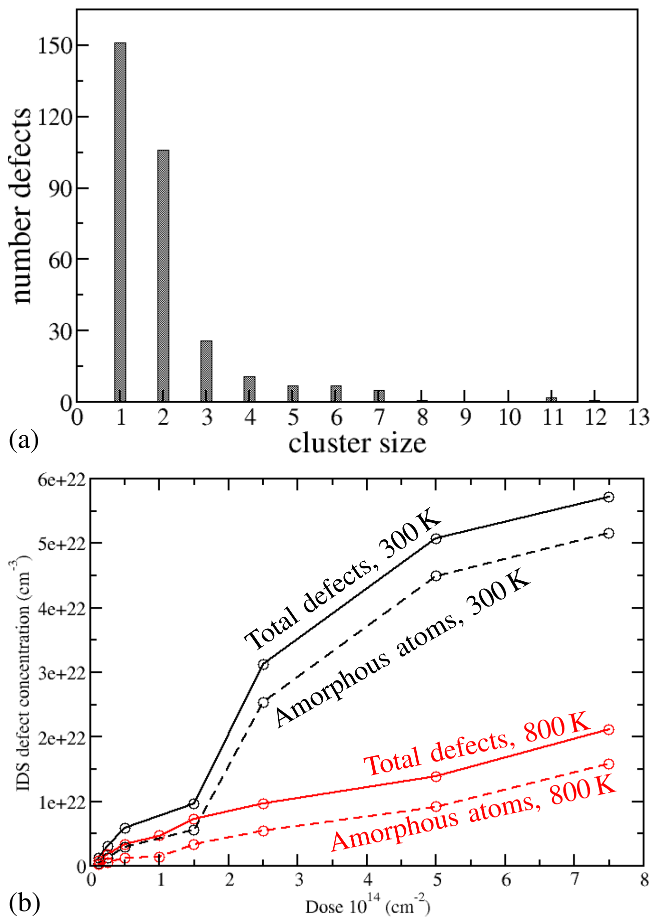

Fig. 4. (a) Defect cluster sizes for the system with an implant dose of $5 \times 10^{13}\,\text{cm}^{-2}$ and temperature of 800 K. (b) IDS defect concentration in the implanted volume respective of implant dose and temperature; dashed lines give the number of atoms in amorphous structures.

IV. Conclusion

From this study, we can conclude that Al implantation in SiC at elevated temperatures is favorable for all doses. Further studies at different doses and temperatures will allow to optimize the achieved activation during annealing. The types and concentrations of defects should be investigated more closely, as well as their influence on the migration and accommodation of the dopant. Longer annealing times will also be studied in order to be able to more directly compare our calculations to experimental results. This would be possible in the high temperatures/low dose regime using a newly developed sampling technique [20], where one can reach system times of up to a few seconds.

Acknowledgement

Financial support by the Federal Ministry of Labour and Economy, the National Foundation for Research, Technology and Development and the Christian Doppler Research Association is gratefully acknowledged.

References

[1] A. Gali *et al.*, "*Ab initio* supercell calculations on aluminum-related defects in SiC," *Phys. Rev. B*, vol. 75, no. 4, p. 045211, Jan. 2007.

[2] J. Chao *et al.*, "Carbon tri-interstitial defect: A model for the D_{II} center," *Phys. Rev. B*, vol. 86, no. 14, p. 144118, Oct. 2012.

[3] A. Y. Kuznetsov *et al.*, "Dynamic annealing in ion implanted SiC: Flux versus temperature dependence," *J. Appl. Phys.*, vol. 94, no. 11, pp. 7112–7115, Dec. 2003.

[4] Y. Zhang *et al.*, "Damage evolution and recovery on both Si and C sublattice in Al-implanted 4H-SiC studied by Rutherford backscattering spectroscopy and nuclear reaction analysis," *J. Appl. Phys.*, vol. 91, no. 10, pp. 6388–6395, 2002.

[5] A. Hallén and M. Linnarsson, "Ion implantation technology for silicon carbide," *Surf. Coat. Technol.*, vol. 306, pp. 190–193, Nov. 2016.

[6] Y. Huang *et al.*, "Kick-out diffusion of Al in 4H-SiC: An ab initio study," *J. Appl. Phys.*, vol. 132, no. 1, p. 015701, Jul. 2022.

[7] H. Yuanchao *et al.*, "Compensation of p-type doping in Al-doped 4H-SiC," *J. Appl. Phys.*, vol. 131, no. 18, p. 185703, May 2022.

[8] A. P. Thompson *et al.*, "LAMMPS - a flexible simulation tool for particle-based materials modeling at the atomic, meso, and continuum scales," *Comput. Phys. Commun.*, vol. 271, p. 108171, Feb. 2022.

[9] A. Stukowski, "Visualization and analysis of atomistic simulation data with OVITO-the Open Visualization Tool," *Model. Simul. Mater. Sci. Eng.*, vol. 18, no. 1, p. 015012, Dec. 2009.

[10] R. Devanathan *et al.*, "Displacement threshold energies in β-SiC," *J. Nucl. Mater.*, vol. 253, no. 1-3, pp. 47–52, Mar. 1998.

[11] F. Gao and W. J. Weber, "Empirical potential approach for defect properties in 3C-SiC," *Nucl. Instrum. Methods Phys. Res. B*, vol. 191, no. 1-4, pp. 504–508, May 2002.

[12] C. R. Dandekar and Y. C. Shin, "Molecular dynamics based cohesive zone law for describing Al–SiC interface mechanics," *Compos. - A: Appl. Sci.*, vol. 42, no. 4, pp. 355–363, Apr. 2011.

[13] N. Matsushima and J. Yamauchi, "First-principles X-ray photoelectron spectroscopy binding energy shift calculation for boron and aluminum defects in 3C-silicon carbide," *Jpn. J. Appl. Phys.*, vol. 58, no. 3, p. 031001, Feb. 2019.

[14] M. Bockstedte *et al.*, "*Ab initio* study of the migration of intrinstic defects in 3C-SiC," *Phys. Rev. B*, vol. 68, no. 20, p. 205201, Nov. 2003.

[15] T. Kobayashi *et al.*, "Native point defects and carbon clusters in 4H-SiC: A hybrid functional study," *J. Appl. Phys.*, vol. 125, no. 12, p. 125701, Mar. 2019.

[16] F. Gao *et al.*, "Atomistic study of intrinsic defect migration in 3C-SiC," *Phys. Rev. B*, vol. 69, no. 24, p. 245205, Jun. 2004.

[17] F. Gao and W. J. Weber, "Recovery of close Frenkel pairs produced by low energy recoils in SiC," *J. Appl. Phys.*, vol. 94, no. 7, pp. 4348–4356, Oct. 2003.

[18] W. Weber *et al.*, "Ion-beam induced defects and nanoscale amorphous clusters in silicon carbide," *Nucl. Instrum. Methods Phys. Res. B*, vol. 216, pp. 25–35, Feb. 2004.

[19] G. Samolyuk *et al.*, "Molecular dynamics modeling of atomic displacement cascades in 3C-SiC: Comparison of interatomic potentials," *J. Nucl. Mater.*, vol. 465, pp. 83–88, Oct. 2015.

[20] K. M. Bal and E. C. Neyts, "Merging Metadynamics into Hyperdynamics: Accelerated molecular simulations reaching time scales from microseconds to seconds," *J. Chem. Theory Comput.*, vol. 11, no. 10, pp. 4545–4554, Sep. 2015.